A NLO calculation of the hadron-jet cross section in photoproduction reactions

M. Fontannaz[1], J.Ph. Guillet[2], G. Heinrich[3]

[1] Laboratoire de Physique Théorique LPT[a], Université de Paris XI, Bâtiment 210, 91405 Orsay, France
[2] Laboratoire d'Annecy-Le-Vieux de Physique Théorique LAPTH[b], Chemin de Bellevue, B.P. 110, 74941 Annecy-le-Vieux, France
[3] Department of Physics, University of Durham, Durham DH1 3LE, UK

Abstract. We study the photoproduction of large p_T charged hadrons in ep collisions, both for the inclusive case and for the case where a jet in the final state is also measured. Our results are obtained by a NLO generator of partonic events. We discuss the sensitivity of the cross section to the renormalisation and factorisation scales, and to various fragmentation function parametrisations. The possibility to constrain the parton densities in the proton and in the photon is assessed. Comparisons are made with H1 data for inclusive charged hadron production.

1 Introduction

The photoproduction of large p_T jets, photons or hadrons are privileged reactions to study QCD and to measure the parton distributions in the proton and in the photon. In the past, the interest was mainly focused on the production of jets [1,2], and more recently on the production of photons [3]. Particularly interesting are the dijet cross sections [4,5], or the photon-jet cross sections [6], because the measurement of two jets or particles in the final state allows one to constrain the incoming parton kinematics and to explore the parton distributions in an accurate way. In this paper we present results concerning the large p_T photoproduction of a charged hadron and a jet, $ep \rightarrow h^{\pm} + \text{jet}$. This reaction offers several interesting features in comparison with dijet or photon-jet reactions. With respect to the latter, the hadron-jet cross section is much higher; the observation of a hadron is also easier than that of a photon. Compared to the dijet reaction, the hadron-jet one is also easier to measure, this fact being particularly true at small p_T (~ 5–$10\,\text{GeV}$) where it is difficult to model the underlying event contribution and to unambiguously measure the transverse momentum of two jets. It should also be possible to explore a larger rapidity domain for the hadron since there is no cone "hitting the edge" of the detector.

These features are important when one focuses on the measurement of the parton distributions in the photon. As is well known, there are two contributions to photo-

production cross sections: the so-called direct and resolved contributions. The resolved contribution is important at small values of p_T and at large positive rapidities, a kinematic domain that the hadron-jet reaction should allow one to explore.

The theoretical description of the hadron-jet cross sections requires the knowledge of the fragmentation functions of quarks and gluons into hadrons. This might appear as a disadvantage with respect to the jet–jet reaction. However one has to note that hadronisation corrections are also needed in jet reactions to describe the evolution of partons into hadrons and they are not totally under control. Moreover fragmentation functions are now well measured in LEP experiments and several recent NLO parametrisations of quark and gluon fragmentation functions are available [7–9]. These fragmentation functions have been tested in inclusive charged hadron production in $p\bar{p}$, γp and $\gamma\gamma$ collisions by Kniehl, Kramer and Pötter in [10]; they found a good agreement between theory and data, which confirms that the fragmentation functions are under control. In this paper we concentrate on the hadron-jet physics and assess the possibility to constrain the parton distribution functions of the photon and of the proton. In jet–jet reactions, it is usual to constrain the momentum of the incoming partons by means of the variables $x_{\text{obs}}^{p,\gamma} = (p_T^{\text{jet}_1} e^{\pm \eta^{\text{jet}_1}} + p_T^{\text{jet}_2} e^{\pm \eta^{\text{jet}_2}})/2E^{p,\gamma}$ and of the variables $x_{\text{LL}}^{p,\gamma} = p_T^{\text{jet}_1}(e^{\pm \eta^{\text{jet}_1}} + e^{\pm \eta^{\text{jet}_2}})/2E^{p,\gamma}$, where $E^{p,\gamma}$ are the energies of the incoming proton respectively photon. (We follow the HERA convention with the proton momentum oriented toward the positive z-axis and the photon momentum toward the negative z-axis.) For the Born contributions, with only two jets in the final

state, the variables $x^{p,\gamma}$ exactly correspond to the longitudinal momentum fractions of the partons in the proton and in the photon. When higher order QCD corrections are considered, the variables $x^{p,\gamma}$ do not fix the initial momenta anymore, but they still put useful constraints on these momenta. The situation is different in the hadron-jet case because the hadron momentum p_T^h is only a fraction of the momentum of the outgoing parton, such that $x^{p,\gamma}$ (with $p_\mathrm{T}^{\mathrm{jet}_1}$ replaced by p_T^h) do not even for the Born cross section correspond to the incoming parton momenta anymore. Therefore it is interesting to study the usefulness of such variables in the hadron-jet case, and how they can help to measure the proton and photon parton distributions. The results presented in this paper are based on a NLO Monte Carlo program which generates events containing 2 or 3 partons in the final state. One of them fragments into a large p_T hadron, and the others are recombined into jets. This NLO event generator provides a flexible approach to implement experimental cuts and to calculate a large variety of observables. The theoretical framework and the Monte Carlo program are presented in Sect. 2. In Sect. 3 we compare theoretical predictions for the inclusive (i.e. no jet observed) cross section with H1 data [11]. The emphasis is put on the study of the sensitivity of the cross section to the factorisation and renormalisation scales, and to different fragmentation function parametrisations. In Sect. 4 we study the hadron-jet cross section and explore the distributions $\mathrm{d}\sigma/\mathrm{d}x^{p,\gamma}$, in particular their sensitivity to the gluon densities in the proton and the photon. Section 5 is the conclusion.

2 Theoretical framework

The NLO Monte Carlo program used in this paper has already been described in [12,13] in which the photoproduction of isolated prompt photons is studied. Therefore we only give a few indications on the general structure of the program here and discuss the new features specific to the photoproduction of hadrons. In photoproduction events, the electron acts like a source of quasi-real photons whose spectrum can be described by the Weizsäcker–Williams formula

$$f_\gamma^e(y) = \frac{\alpha_\mathrm{em}}{2\pi}$$
$$\times \left\{ \frac{1 + (1-y)^2}{y} \ln \frac{Q^2_\mathrm{max}(1-y)}{m_e^2 y^2} - \frac{2(1-y)}{y} \right\}. \quad (1)$$

The quasi-real photon then either takes part *directly* in the hard scattering process, or it acts as a composite object, being a source of partons which take part in the hard subprocess. The latter mechanism is referred to as a *resolved* process and is parametrised by the photon structure functions $F_{a/\gamma}(x_\gamma, Q^2)$. Thus the distribution of partons in the electron is a convolution

$$F_{a/e}(x_e, M) = \int_0^1 \mathrm{d}y \mathrm{d}x_\gamma f_\gamma^e(y) F_{a/\gamma}(x_\gamma, M)$$
$$\times \delta(x_\gamma y - x_e), \quad (2)$$

where in the "direct" case $F_{a/\gamma}(x_\gamma, M) = \delta_{a\gamma}\delta(1 - x_\gamma)$. The production of the final hadron h with momentum P_h is described by a fragmentation function $D_a^h(z, M_F)$, where z is the fraction of the longitudinal momentum of the parton a carried away by the hadron h. The production cross section of a large p_T hadron and a jet is written as a convolution of the distributions of initial partons, the fragmentation of the final parton and the hard scattering cross sections

$$\mathrm{d}\sigma^{ep\to h\mathrm{jet}}(P_p, P_e, P_h, P_\mathrm{jet}) = \sum_{a,b,c} \int \mathrm{d}x_e \int \mathrm{d}x_p \int \mathrm{d}z$$

$$\times F_{a/e}(x_e, M) F_{b/p}(x_p, M) D_c^h(z, M_F)$$
$$\times \mathrm{d}\widehat{\sigma}^{ab\to c\mathrm{jet}}(x_p P_p, x_e P_e, P_h/z, P_\mathrm{jet}, \mu, M, M_F). \quad (3)$$

The hard cross sections $\mathrm{d}\widehat{\sigma}^{ab\to c\mathrm{jet}}$ are calculated at the NLO accuracy. They are expansions in powers of $\alpha_\mathrm{s}(\mu)$

$$\mathrm{d}\widehat{\sigma}^{\gamma b\to c\mathrm{jet}} = \alpha_\mathrm{s}(\mu)\mathrm{d}\widehat{\sigma}_\mathrm{BORN}^{\gamma b\to c\mathrm{jet}}$$
$$+ \alpha_\mathrm{s}^2(\mu)\mathrm{d}\widehat{\sigma}_\mathrm{HO}^{\gamma b\to c\mathrm{jet}}(\mu, M, M_F) + \mathcal{O}(\alpha_\mathrm{s}^3), \quad (4)$$

$$\mathrm{d}\widehat{\sigma}^{ab\to c\mathrm{jet}} = \alpha_\mathrm{s}^2(\mu)\mathrm{d}\widehat{\sigma}_\mathrm{BORN}^{ab\to c\mathrm{jet}}$$
$$+ \alpha_\mathrm{s}^3(\mu)\,\mathrm{d}\widehat{\sigma}_\mathrm{HO}^{ab\to c\mathrm{jet}}(\mu, M, M_F) + \mathcal{O}(\alpha_\mathrm{s}^4). \quad (5)$$

In expressions (3), (4) and (5), we have explicitly written the dependence on the large scales μ, M and M_F. (For simplicity we choose the same factorisation scale M for the incoming photon and proton.) The cross section (3) would not depend on these large scales if it were calculated to all orders in $\alpha_\mathrm{s}(\mu)$. But after truncation of the series (4) and (5), the cross section will depend on μ, M and M_F. The μ-, M- and M_F-dependence of the HO terms partially compensates the scale dependence of the Born cross sections, and in the next sections we shall study the sensitivity of $\mathrm{d}\sigma^{ep\to h\mathrm{jet}}$ to the renormalisation scale μ and the factorisation scales M and M_F.

Let us now discuss the various components of formula (3). The fragmentation functions $D_a^h(z, M_F)$ have been accurately measured in LEP experiments and several NLO parametrisations of the latter are now available [7–9]. There exist non-negligible differences between the parametrisations of individual $D_a^h(z, M_F)$, especially at large $z \gtrsim 0.8$, but for cross sections involving sums over the flavours a and over the hadrons h the differences are tiny. In photoproduction, the weights of the different flavours which contribute to the cross section are identical to those of the e^+e^--annihilation reaction (at least for the direct contribution). Therefore the differences between the individual contributions should be smoothed when summed over to form the cross section. In the next section we shall check the sensitivity of the photoproduction cross section to the fragmentation functions. We now turn to another important component of formula (3), the quark and gluon distributions in the photon. In this paper we use a new NLO parametrisation of these distributions, the AFG02 parametrisation [14]. The AFG02 parametrisation is an evolution of the AFG [15] parametrisation. The new distributions are more flexible: for instance the shape and normalisation of the non-perturbative gluon distribution can

be modified. This fact allows one to study the sensitivity of cross sections to the gluon distribution. The normalisation of the non-perturbative quark distributions can also be adjusted. Contrary to the AFG distributions, the AFG02 distributions also contain the bottom quark distribution. In this paper we shall use the default AFG02 parametrisation which is almost identical to the AFG parametrisation; the only differences are the number of flavours and the value of $\Lambda_{\overline{MS}}^{(4)} = 300\,\text{MeV}$ ($\Lambda_{\overline{MS}}^{(4)} = 200\,\text{MeV}$ was used in the AFG parametrisation in agreement with the value of $\Lambda_{\overline{MS}}^{(4)}$ determined ten years ago). As a result, due to a faster QCD evolution, the AFG02 distributions are slightly higher at small x and lower at large x than the AFG distributions.

For the parton distributions in the proton, we use MRST99 (g↑) [24] as default. For the hadron-jet cross section, we will also use the new MRST01 [25] and CTEQ6M [26] sets for comparison.

We use a strong coupling constant calculated by solving exactly (i.e. without expansion in $\log Q^2/\Lambda^2$) the two-loop renormalisation group equation. We work with $N_f = 4$ active flavours as default. Using $N_f = 5$ the total cross section increases by about 5%.

Expression (3) is calculated via a MC code which generates $2 \to 2$ and $2 \to 3$ parton configurations according to weights given by the subprocess cross sections and the distribution functions. A phase space slicing method is used to isolate and to analytically calculate the soft and collinear singular contributions of the $2 \to 3$ cross sections. The soft divergences are cancelled by the corresponding divergences contained in the virtual corrections to the $2 \to 2$ processes (UV divergences are removed by renormalisation in the $\overline{MS}$ scheme). The remaining collinear singularities are factored out and absorbed in the distribution and fragmentation functions using the $\overline{MS}$ scheme. This Monte Carlo code, which uses the event generator Bases/Spring [16], is a partonic event generator: it contains negative weights coming for instance from the virtual corrections to the Born cross sections. It is very flexible and allows one to study various cross sections involving a large p_T hadron and jets. Experimental cuts are easily taken into account, as well as different jet algorithms. In this paper, we use the k_T-algorithm [17] to define the jets.

3 Large-p_T hadron inclusive cross section

In this section we study the photoproduction of large p_T inclusive hadrons. Similar studies and comparisons with data have already been performed in several publications [10,18–20]. Therefore we shall not carry out an exhaustive study of this reaction, but we shall concentrate on the sensitivity of the cross section to the factorisation and renormalisation scales, and to different parametrisations of the fragmentation functions. In Fig. 1, we display a study of the scale dependence. The theoretical curves are compared to H1 data [11] corresponding to the following kinematic conditions. The parameters of the Weizsäcker–Williams formula are $Q^2_{max} = 0.01\,\text{GeV}^2$ and $0.3 \leq y \leq 0.7$. The ep center of mass energy is $S_{ep}^{1/2} = 300\,\text{GeV}$. The cross
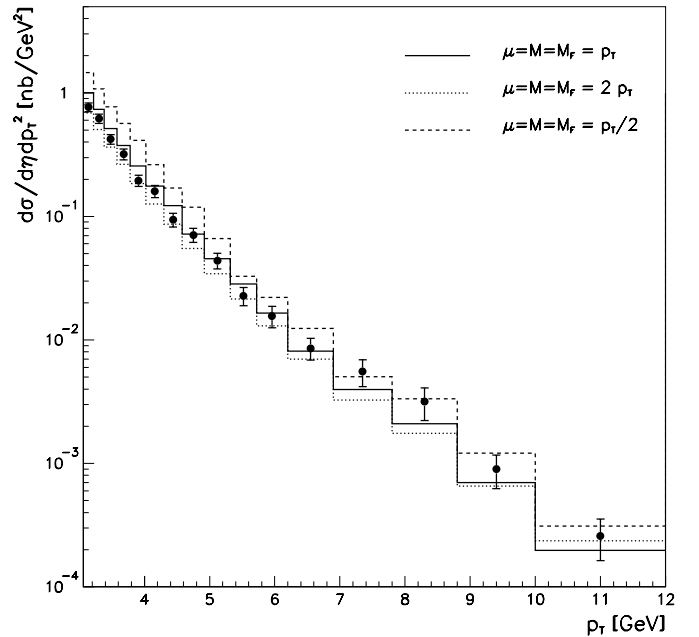
Fig. 1. $d\sigma/d\eta dp_T^2$ for 3 different scale choices compared to H1 data

section for large p_T charged hadrons is measured in the pseudo-rapidity domain $|\eta| \leq 1$. The theoretical curves are obtained with the BFGW fragmentation functions [9] and we use $\Lambda_{\overline{MS}}^{(4)} = 300\,\text{MeV}$.

We can see from Fig. 1 that the data are described fairly well, in particular that no intrinsic k_T is needed to describe the data at low p_T, contrary to what has been found in the E706 experiment on fixed target inclusive π^0 production [21,22].

In Fig. 2 we show on a linear scale the ratios of the cross sections calculated with $M = M_F = \mu = Cp_T$ ($C = 0.5, 2$) to the cross section calculated at $C = 1$, where p_T is the transverse momentum of the final state hadron. Results obtained with the KKP [8] fragmentation function parametrisations are also displayed[1].

We clearly see a strong dependence of the cross section on the scales for $p_T \lesssim 7\,\text{GeV}$. Below 7 GeV the perturbative calculation is not reliable, the HO corrections being very large. Moreover, for the choice $C = 1/2$ we explore a range of the factorisation scales ($M = M_F = p_T/2 \sim 1.5\,\text{GeV}$) which is very far from the kinematic region where the fragmentation functions have been constrained.

We also find a strong scale dependence of the rapidity distribution $d\sigma/d\eta$ which is measured in the range $3\,\text{GeV} \leq p_T \leq 12\,\text{GeV}$. In Table 1 we give the results of a study of $\Delta\sigma = \int_0^{.5} d\eta(d\sigma/d\eta)$ in which we separately

---

[1] The dip at $p_T \sim 5\,\text{GeV}$ in the KKP ratio may stem from the fact that the charm threshold is at $M_F = 2m_c$ in these parametrisations. Therefore there is no charm contribution below $p_T \sim 6\,\text{GeV}$ in the case $C = 0.5$, whereas for $C = 1$ the charm contributes already at 3 GeV. In the BFGW parametrisations the charm threshold is at $M_F = m_c$, such that the charm contributes at $p_T \geq 3\,\text{GeV}$ even for $C = 0.5$
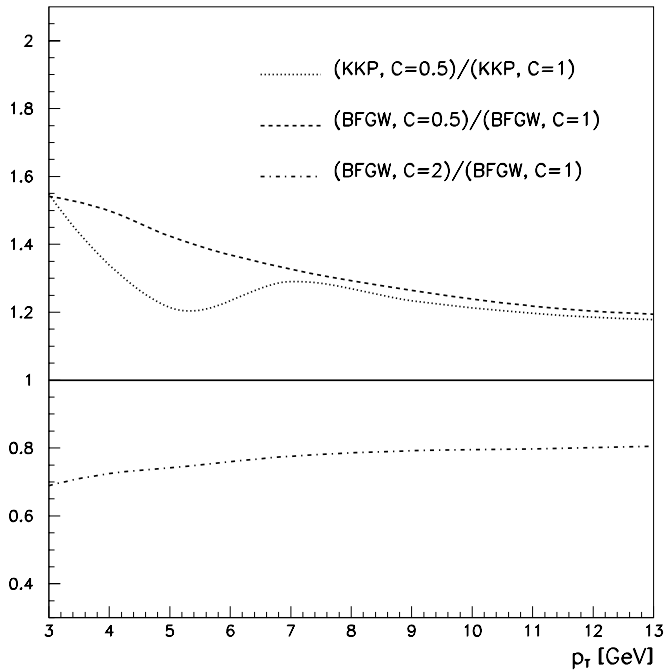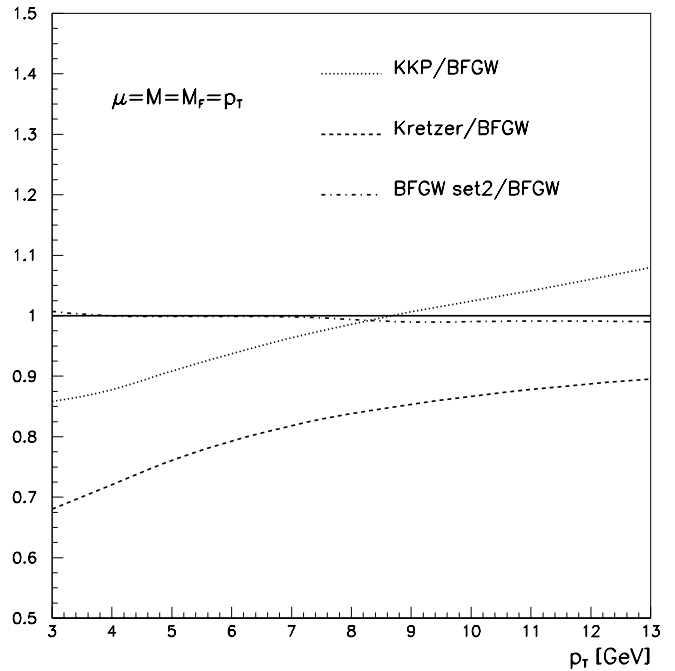
Fig. 2. $d\sigma/dp_T$ calculated with scales $\mu = M = M_F = Cp_T$ ($C = 0.5, 2$) normalised to $d\sigma/dp_T$ at $\mu = M = M_F = p_T$
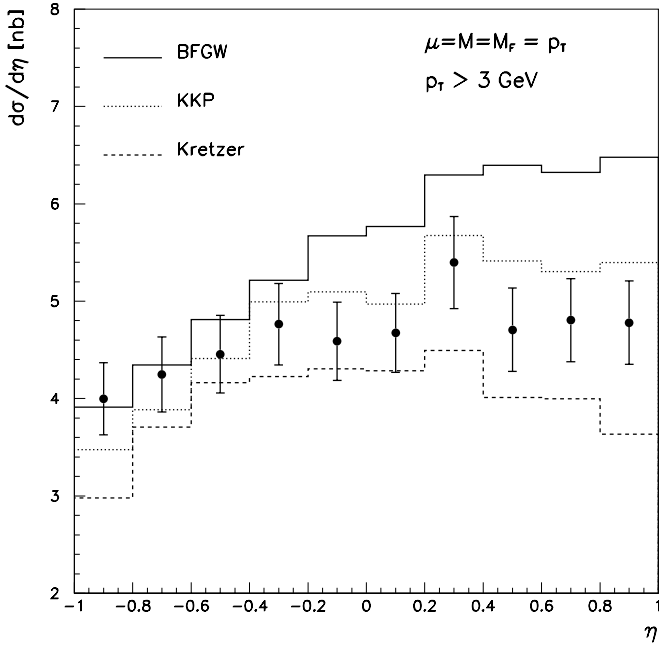

Fig. 3. $d\sigma/dp_T$ with different fragmentation functions normalised to $d\sigma/dp_T$ with BFGW (set 1) fragmentation functions, at the scales $\mu = M = M_F = p_T$ and the hadron rapidity integrated over the range $|\eta| < 1$

Table 1. μ, M-dependence of the total cross section integrated over $0 \leq \eta \leq 0.5$ and $3\,\text{GeV} < p_T < 12\,\text{GeV}$. The fragmentation scale has been kept fixed to $M_F = p_T$. The bold numbers denote the total cross section in nb, the numbers in italic represent the ratio $r = \text{HO}/(\text{Born} + \text{HO})$. One can see that there is no region of stability for a value of p_T^{min} as low as 3 GeV

	C_M	0.5	1	2
$C_\mu = 0.5$	σ	**3.941**	**4.509**	**4.807**
	r	*(0.54)*	*(0.42)*	*(0.31)*
$C_\mu = 1$	σ	**2.580**	**3.079**	**3.430**
	r	*(0.57)*	*(0.48)*	*(0.41)*
$C_\mu = 2$	σ	**1.855**	**2.264**	**2.564**
	r	*(0.58)*	*(0.52)*	*(0.46)*

vary μ and M, keeping fixed $M_F = p_T$. The upper number is the total cross section (direct + resolved) and the lower number is the ratio $r = \text{HO}/(\text{Born} + \text{HO})$. The variation of the cross section with $C_\mu = \mu/p_T$ is very strong for small values of C_μ ($C_\mu \sim 0.5$) corresponding to large values of $\alpha_s(\mu)$. There is no region where the cross section $\sigma(C_M, C_\mu)$ is almost independent of C_M and C_μ, and the ratio r is always large. We again conclude that the theoretical predictions are not reliable for $p_T \sim 3\,\text{GeV}$, a p_T-region which gives an important contribution to the cross section integrated over $3\,\text{GeV} \leq p_T \leq 12\,\text{GeV}$.

The situation improves when we study the sensitivity to scale changes for larger values of p_T. For instance at $p_T = 7\,\text{GeV}$ – although the sensitivity is still large when we vary all scales by the same factor C (see Fig. 2) – we find a region where the cross section as a function of M and μ has a flat behaviour. We can see from Table 2,

Table 2. μ, M-dependence of the total cross section integrated over $|\eta| \leq 1$ at $p_T = 7\,\text{GeV}$. The fragmentation scale has been fixed to $M_F = p_T/2$. The bold numbers denote the total cross section in nb, the numbers in italic represent the ratio $r = \text{HO}/(\text{Born} + \text{HO})$. In this case there is a rather flat region for small values of μ and large values of M, and the overall variation of the cross section due to scale changes is much smaller

	C_M	0.3	0.5	1	2
$C_\mu = 0.3$	σ	**0.254**	**0.243**	**0.229**	**0.224**
	r	*(0.25)*	*(0.06)*	*(-0.19)*	*(-0.40)*
$C_\mu = 0.5$	σ	**0.220**	**0.222**	**0.223**	**0.228**
	r	*(0.38)*	*(0.27)*	*(0.13)*	*(0.03)*
$C_\mu = 1$	σ	**0.176**	**0.184**	**0.192**	**0.200**
	r	*(0.45)*	*(0.38)*	*(0.29)*	*(0.23)*

where M_F is kept fixed to $p_T/2$, that there is a stability region for $0.3 \lesssim C_\mu \lesssim 0.5$ and $0.5 \lesssim C_M \lesssim 2$. Fixing $\mu = 0.4p_T$ and $M = 1.5p_T$ at the saddle point of the surface given in Table 2, we also studied the dependence on M_F and found that the cross section varies by $\pm 2\%$ when M_F is varied between $0.3p_T$ and p_T. Therefore the scale sensitivity appears to be under control for large values of p_T ($p_T \gtrsim 7\,\text{GeV}$). We shall pursue this study in the next section for the hadron-jet cross section.
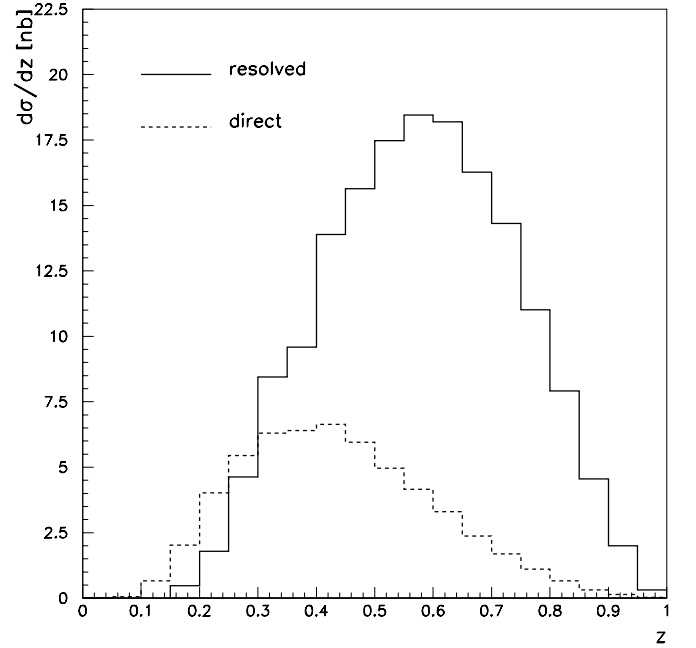
The sensitivity to the fragmentation function parametrisations [7–9] is less pronounced than the one due to scale variations. This result is illustrated in Fig. 3. For $p_T > 7\,\text{GeV}$, there is at most a 20% difference between the

Fig. 4. $d\sigma/d\eta$ with different sets of fragmentation functions compared to H1 data

Fig. 5. Distribution of the hadron momentum fraction z for the direct and resolved contributions. ($3\,\mathrm{GeV} \leq p_\mathrm{T} \leq 12\,\mathrm{GeV}$, $|\eta| < 1$, $\mu = M = M_F = p_\mathrm{T}$.)

various parametrisations, the BFGW and KKP parametrisations being quite close to each other. The BFGW set 2 parametrisation has a slightly higher gluon than the default BFGW for $0.2 \lesssim z \lesssim 0.6$ and a lower gluon for $z \gtrsim 0.6$, due to a higher N_g in the input parameter set. Since the HERA kinematics do not probe high z values, the difference with the BFGW default set is negligible in our case, as can be seen from Fig. 3. However, the sensitivity to the fragmentation functions is non-negligible for $p_\mathrm{T} \sim 3\,\mathrm{GeV}$, a range explored by H1. In Fig. 4 we display a comparison between H1 data and theoretical results obtained with different sets of fragmentation functions. The dispersion of the results is quite large. In this regard it is instructive to look at the distribution $d\sigma/dz$, which is not a physical quantity (the momentum of the parton "parent" of the hadron h cannot be measured), but which gives interesting indications on the average value $\langle z \rangle$ in the cross section, and on the variance $\langle z^2 \rangle - \langle z \rangle^2$. The z-distributions are displayed in Fig. 5 for the direct and resolved components. One can see that two different ranges in z of the fragmentation functions are probed by the direct respectively resolved component. The mean value $\langle z \rangle$ is larger for the resolved contribution[2]. Since the various fragmentation function parametrisations differ mostly at high z, a change of parametrisation will have a different effect on the direct and on the resolved contribution. This effect can be seen in Fig. 4, where we observe that the

differences between the various parametrisations are more pronounced for positive rapidities, a region corresponding to a large resolved contribution. We again verify in Fig. 4 that the value of $p_\mathrm{T}^{\min} = 3\,\mathrm{GeV}$ is too small to allow for a reliable prediction, the dispersion of the results for the various parametrisations being too large at low p_T.
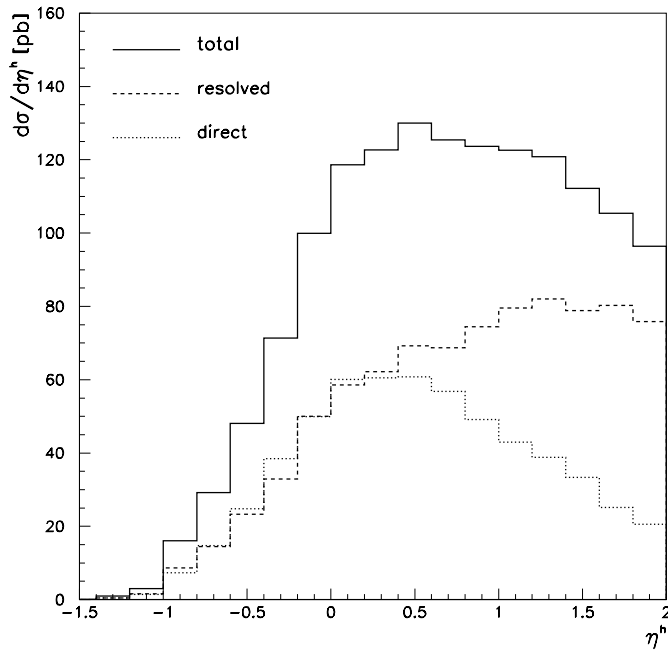
We further investigated the impact of using an expansion in $\log Q^2/\Lambda^2$ for α_s instead of the numerical solution of the two-loop renormalisation group equation, and found the result being about 10% lower when using the expansion in $\log Q^2/\Lambda^2$. We also compared our result to the one of Kniehl, Kramer and Pötter [10]. Using the KKP fragmentation functions and the expansion in $\log Q^2/\Lambda^2$ for α_s, we obtain the result given in [10] within the numerical errors.

4 Hadron-jet cross section

In this section we explore the features of the hadron-jet cross section. The input parameters are the same as for the inclusive cross section, and we consider the cross section $d\sigma/d\eta^h d\eta^{\mathrm{jet}}$ (where η^h is the pseudo-rapidity of the observed charged hadron), integrated in the range $7\,\mathrm{GeV} \leq p_\mathrm{T}^h \leq 15\,\mathrm{GeV}$ and $E_\mathrm{T}^{\mathrm{jet}} > 5\,\mathrm{GeV}$. When there are two jets in the final state, we consider the jet of higher E_T. The jets are defined by the k_T-algorithm with the Snowmass merging rule.

We shall also study the cross sections $d\sigma/dx^{p,\gamma}$, the variables $x^{p,\gamma}$ being either the x_{obs} variables

$$x_{\mathrm{obs}}^{p,\gamma} = \frac{p_\mathrm{T}^h \mathrm{e}^{\pm \eta^h} + E_\mathrm{T}^{\mathrm{jet}}\, \mathrm{e}^{\pm \eta^{\mathrm{jet}}}}{2E^{p,\gamma}} \qquad (6)$$

---

[2] This is due to the fact that the cross section for the production of partons behaves like $d\sigma/dp_\mathrm{T}^{\mathrm{parton}} \sim A/(p_\mathrm{T}^{\mathrm{parton}})^n$ ($n > 0$), such that, using $p_\mathrm{T}^{\mathrm{parton}} = p_\mathrm{T}^h/z$, the behaviour of the cross section is $d\sigma/dz \sim z^{n-2}$ convoluted with the fragmentation functions which decrease with increasing z. The value of n is larger for the resolved part, leading to a larger value of $\langle z \rangle$

Fig. 6. Rapidity distribution for the hadron-jet cross section $d\sigma/d\eta^h$ at the scales $\mu = M = M_F = p_T$, integrated over $7\,\text{GeV} \leq p_T \leq 15\,\text{GeV}$, $E_T^{\text{jet}} \geq 5\,\text{GeV}$, $|\eta^{\text{jet}}| \leq 2$

or the x_{LL} variables

$$x_{\text{LL}}^{p,\gamma} = \frac{p_T^h(e^{\pm\eta^h} + e^{\pm\eta^{\text{jet}}})}{2E^{p,\gamma}}. \tag{7}$$

$E^{p,\gamma}$ are the energies of the incoming proton respectively photon and the plus sign in $e^{\pm\eta}$ corresponds to x^p, the minus sign to x^γ. The main difference between x_{obs} and x_{LL} consists in the fact that the definition of x_{LL} does not require the measurement of the jet transverse energy. Further it has to be noted that – contrary to the dijet cross section – the variables defined in (6) and (7) do not even for the Born contribution coincide with the variables x_{parton}^γ and x_{parton}^p in the parton densities of the photon and the proton. The latter are (for the Born contribution) given by

$$x_{\text{parton}}^{p,\gamma} = \frac{p_T^h}{z}\frac{(e^{\pm\eta^h} + e^{\pm\eta^{\text{jet}}})}{2E^{p,\gamma}}. \tag{8}$$

Therefore the partonic variables $x_{\text{parton}}^{p,\gamma}$ are larger by a factor $1/z$ than the variables $x_{\text{LL}}^{p,\gamma}$, and larger by a factor $(e^{\pm\eta^h} + e^{\pm\eta^{\text{jet}}})/(ze^{\pm\eta^h} + e^{\pm\eta^{\text{jet}}})$ than the variables $x_{\text{obs}}^{p,\gamma}$. At NLO, where a third parton in the final state is involved, the situation is more complicated.

The variables $x_{\text{obs}}^{p,\gamma}$ and $x_{\text{LL}}^{p,\gamma}$ defined in (6) and (7) differ by about $x_{\text{obs}}^{p,\gamma}/x_{\text{LL}}^{p,\gamma} \sim (z+1)/2z$ at central rapidities. This difference will be discussed below in the context of Figs. 8 and 9.

Figure 6 displays the direct and resolved contributions, calculated with the scales $\mu = M = M_F = p_T$, as a function of η^h, integrated over $|\eta^{\text{jet}}| \leq 2$. The two contributions are comparable, except in the forward region where the resolved one is much larger. However, we must keep in
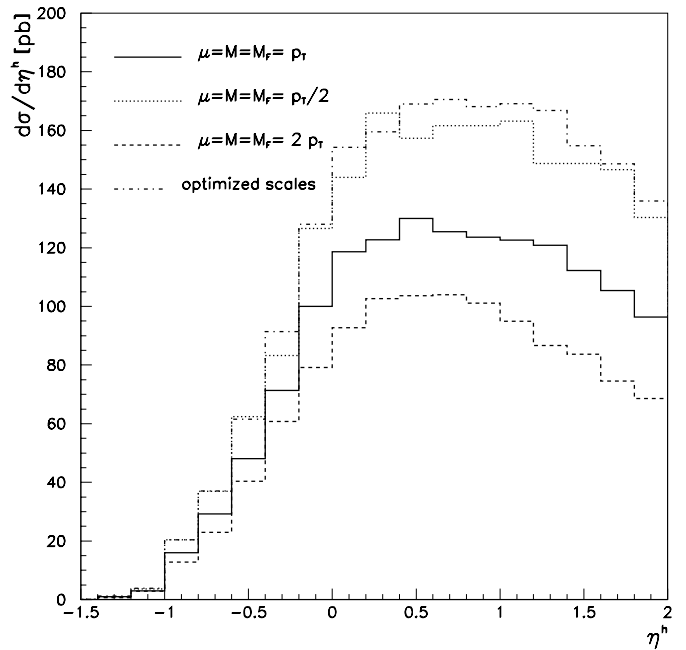
**Fig. 7.** Scale dependence of $d\sigma/d\eta^h$ ($|\eta^{\text{jet}}| \leq 2$)

Table 3. Scale optimisation for the hadron-jet cross section integrated over $0.5 \leq \eta^h \leq 1$, $|\eta^{\text{jet}}| \leq 2$, $7\,\text{GeV} \leq p_T \leq 15\,\text{GeV}$ and $E_T^{\text{jet}} > 5\,\text{GeV}$

| C_{M_F}	C_μ^{opt}	C_M^{opt}	$d\sigma/d\eta^h$ [nb]
1	~ 0.21	~ 1	0.182
0.5	~ 0.3	~ 1.5	0.173
0.3	~ 0.3	~ 1.5	0.180

mind that the pattern of the separate contributions to the cross section depends on the choice of the scales μ, M and M_F; only the sum of the resolved and direct contributions has a physical meaning and can be compared to data.

In Fig. 7 we display the scale dependence of the cross section $d\sigma/d\eta^h$ by varying all scales simultaneously, $\mu = M = M_F = Cp_T$, with the parameter C in the range $1/2 \leq C \leq 2$. We see variations which are similar to those observed in Fig. 2 in the inclusive case for $p_T \sim 7\,\text{GeV}$, where the cross section varies between $+30\%$ and -20% for $1/2 \leq C \leq 2$. However, varying all three scales in the same way is a very rough measure of the scale dependence. A better study has been given in Table 2 where we showed that the cross section exhibits a plateau in the scales μ and M for $0.3 \lesssim C_\mu \lesssim 0.5$ and $0.5 \lesssim C_M \lesssim 2$. We performed a similar investigation for the hadron-jet cross section with the kinematic conditions of Fig. 7. However, contrary to the preceding study, we look for an optimum of the cross section in all three scales μ, M and M_F. That is, we look for optimal scales where $d\sigma/d\mu = d\sigma/dM = d\sigma/dM_F = 0$ [23]. We performed this complete study for $d\sigma/d\eta^h$ with η^h in the range $0.5 \leq \eta^h \leq 1$. The results are displayed in Table 3.

This investigation is very CPU time consuming. Therefore, for a study of the optimum of $d\sigma/d\eta^h$ in various bins
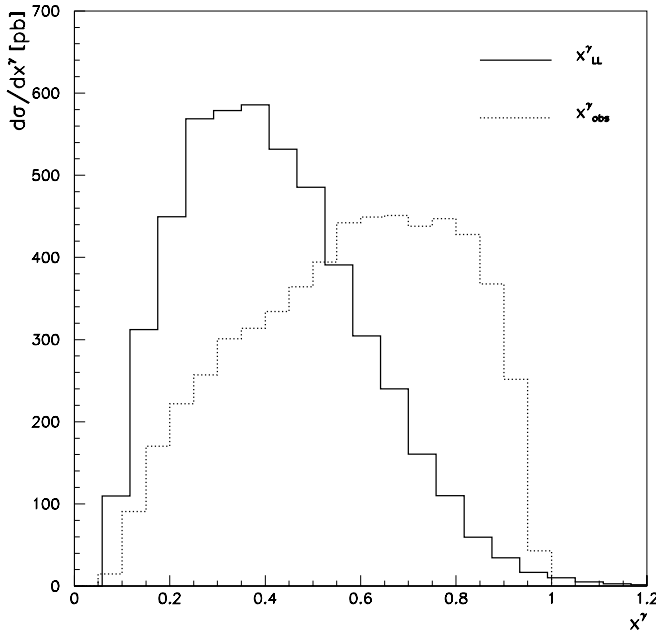
Fig. 8. Comparison of $d\sigma/dx_{obs}^{\gamma}$ and $d\sigma/dx_{LL}^{\gamma}$, integrated over $7\,\mathrm{GeV} \leq p_T \leq 15\,\mathrm{GeV}$, $E_T^{jet} \geq 5\,\mathrm{GeV}$, $|\eta^{jet,h}| < 2$
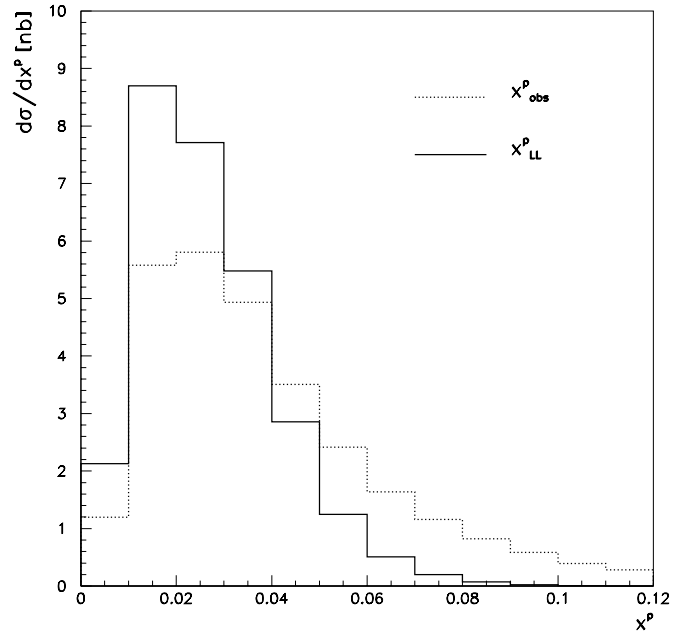
Fig. 9. Comparison of $d\sigma/dx_{obs}^{p}$ and $d\sigma/dx_{LL}^{p}$, integrated over $7\,\mathrm{GeV} \leq p_T \leq 15\,\mathrm{GeV}$, $E_T^{jet} \geq 5\,\mathrm{GeV}$, $|\eta^{jet,h}| < 2$

in η^h, we used the following simplified approach. We fix the scale M_F to the optimal value of Table 3, $M_F = 0.5p_T$, and look for optima of $d\sigma/d\eta^h$ in the (C_μ, C_M)-plane for the η^h bins of Fig. 7. The corresponding cross section is shown in Fig. 7 and we see that it is close to the cross section obtained with $\mu = M = M_F = p_T/2$. It is encouraging to note that the data of Fig. 1 are in good agreement with theory calculated with $C = 0.5$ in the range $p_T > 7\,\mathrm{GeV}$.

Let us now discuss the cross sections $d\sigma/dx_{obs}$ and $d\sigma/dx_{LL}$. Features of these cross sections are displayed in Figs. 8 to 14. Figure 8 gives a clear illustration of the differences between the variables $d\sigma/dx_{obs}$ and $d\sigma/dx_{LL}$. In the partonic variable x_{parton}^{γ} (see (8)), the cross section would have a peak at $x_{parton}^{\gamma} \sim 1$, mainly due to the direct Born contribution which is proportional to $\delta(1 - x_{parton}^{\gamma})$. This peak is shifted to lower values of x_{LL}^{γ} and x_{obs}^{γ} due to the relation $p_T^h = zp_T^a$, where a is the "parent" parton of the hadron h. This shift is larger for the variable x_{LL}^{γ}, as discussed at the beginning of this section. We observe a similar, but much less pronounced pattern for the proton variable x^p; the partonic distributions in the proton decrease rapidly with x_{parton}^p and this behaviour is reflected in the distributions of Fig. 9, $d\sigma/dx_{LL}^p$ having a smaller width than $d\sigma/dx_{obs}^p$.

Figure 10 displays a detailed study of the resolved and direct contributions as functions of x_{LL}^{γ} and x_{obs}^{γ}. As already remarked, the shift of the peak to lower values of x^γ is more pronounced for x_{LL}^{γ} than for x_{obs}^{γ}. The effect of cuts in η^h and η^{jet} are also clearly visible, the kinematic region $0 \leq \eta^h, \eta^{jet} \leq 2$ contributing to the low x^γ domain, and the region $-2 \leq \eta^h, \eta^{jet} \leq 0$ to the large x^γ domain. The relative size of the resolved and direct contributions as

given in Fig. 10 is of course dependent on the scale choice ($\mu = M = M_F = p_T$ for Fig. 10). As already stated at the beginning of this section, only the total cross section is a physical observable. The variation of the size of the direct and resolved contributions with the scales varied by the factor C is shown in Fig. 11. For instance, we observe that for $0.5 \leq C \leq 1$ the resolved component is almost stable, whereas the direct component strongly varies.

The hadron-jet cross section offers the possibility to measure the parton distributions in the proton and in the photon. The quark distributions are constrained by DIS experiments (very well in the proton case, and with rather large errors in the photon case). Therefore, concerning the quark distributions, the hadron-jet cross section can only put some additional constraints on $F_{a/\gamma}(x, M)$. The situation with respect to the gluon distribution is different. The gluon distributions are not well determined in DIS experiments because the virtual photon couples at leading order only to quarks, such that the gluon distributions appear only at the level of higher order corrections. This is not the case for the hadron-jet cross section where the gluon distributions appear already at the Born level. Therefore we expect an important sensitivity of the cross section to the gluon distributions, especially in the kinematic regions where x_{parton} is small. This point is illustrated in Figs. 12 to 14.

In Fig. 12, we observe that the gluon in the photon makes a large contribution at small x^γ, $x^\gamma \lesssim 0.25$. However, the cross section is small in this x^γ-region because the cuts $\eta^h \leq 2$ and $\eta^{jet} \leq 2$ forbid one to reach low values of x^γ. Using different cuts which reinforce the small x^γ-region, namely $1 \leq \eta^h, \eta^{jet} \leq 3$, we obtain the results shown in Fig. 13. We see that the cross section in the small x^γ-region is much larger and made up almost entirely by
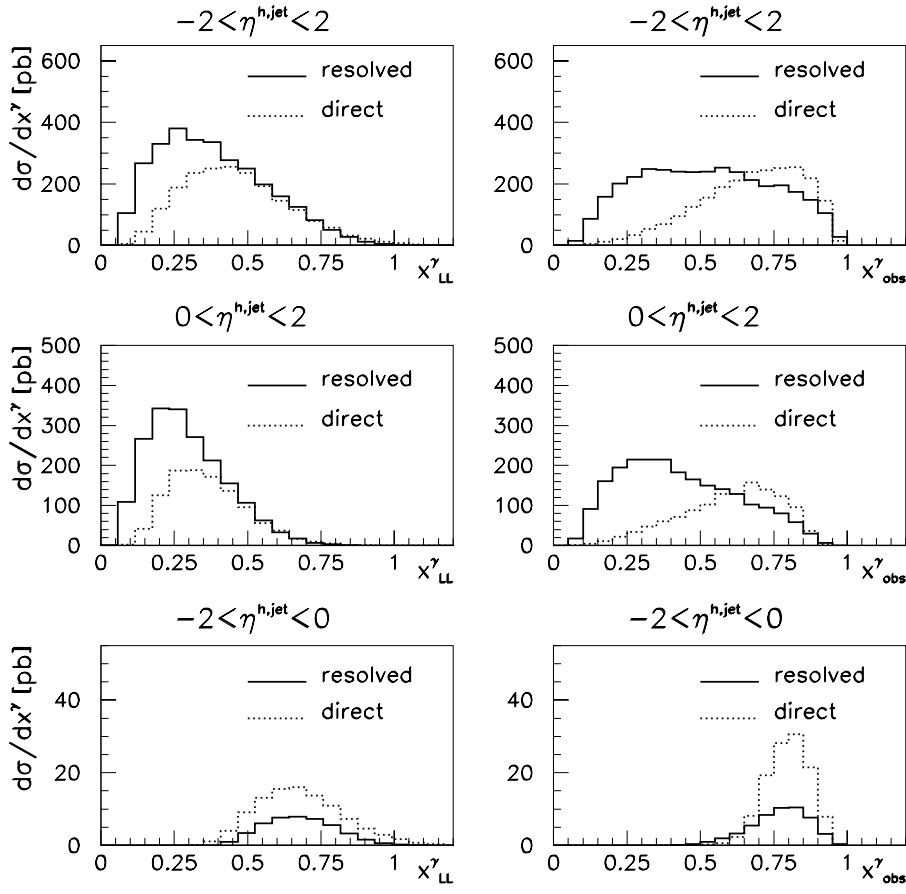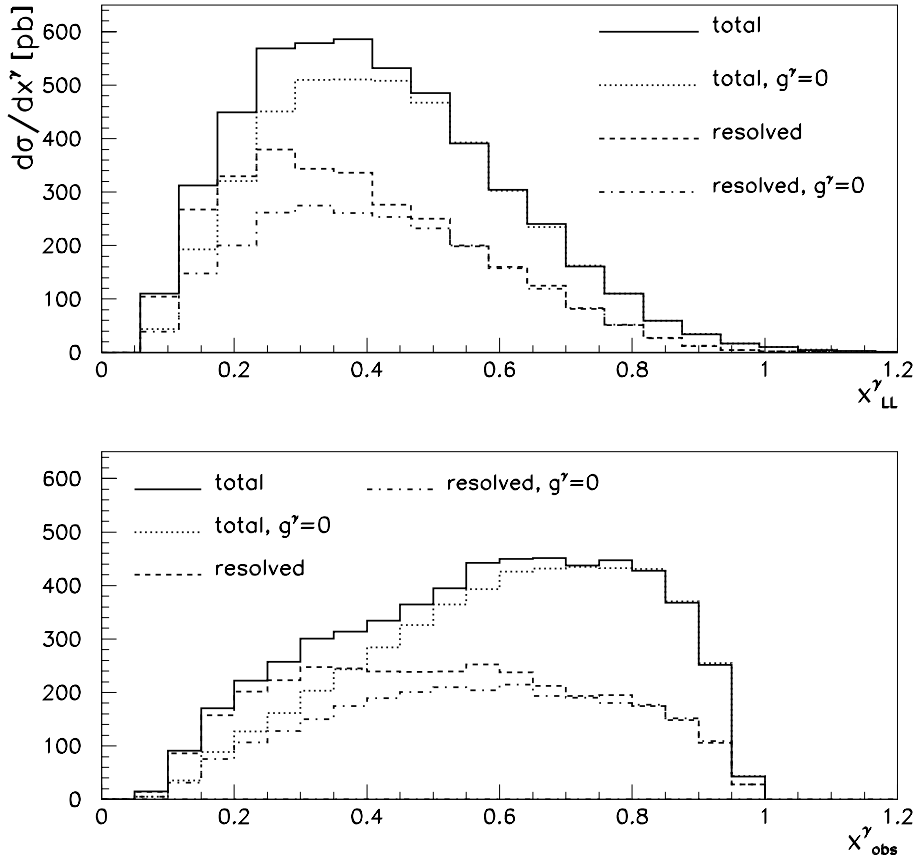
Fig. 10. Comparison of resolved and direct contributions to $\mathrm{d}\sigma/\mathrm{d}x^{\gamma}_{\mathrm{obs}}$ and $\mathrm{d}\sigma/\mathrm{d}x^{\gamma}_{\mathrm{LL}}$ in different rapidity ranges
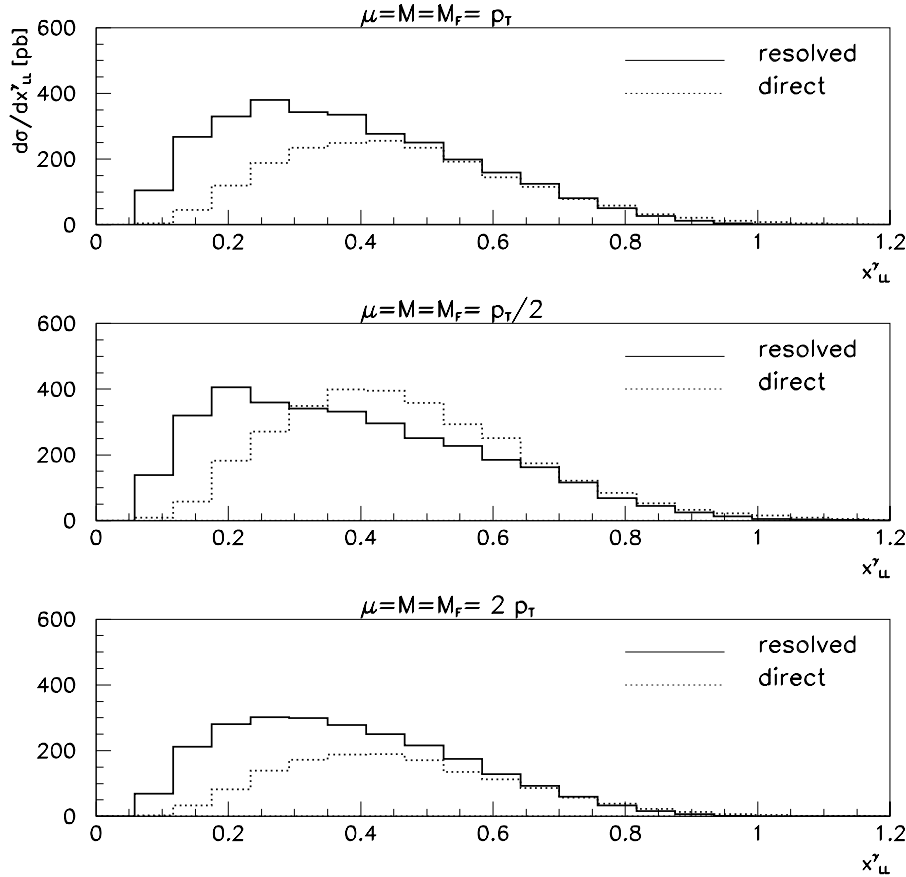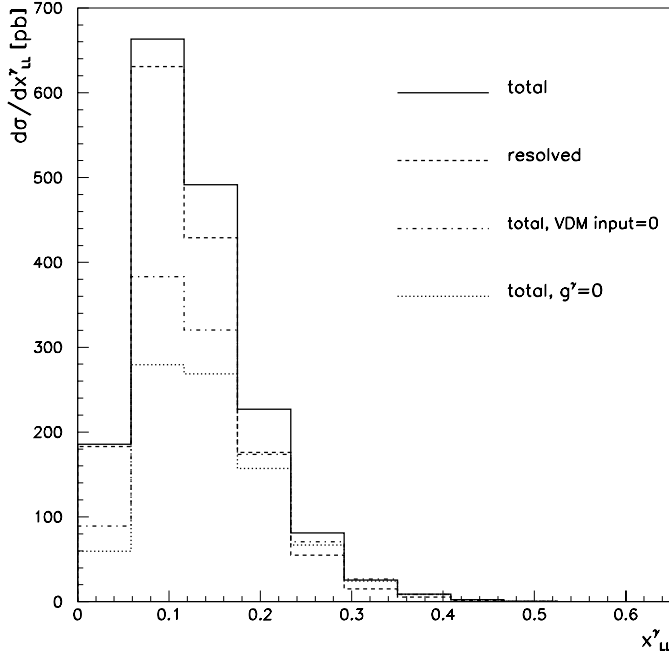

Fig. 11. Comparison of resolved and direct parts for different scale choices, integrated over the rapidity range $-2 \leq \eta^{h,\mathrm{jet}} \leq 2$

Fig. 12. Contribution of the gluon in the photon to $\mathrm{d}\sigma/\mathrm{d}x_{\mathrm{obs}}^{\gamma}$ and $\mathrm{d}\sigma/\mathrm{d}x_{\mathrm{LL}}^{\gamma}$. The rapidities are integrated over the range $-2 \le \eta^{h,\mathrm{jet}} \le 2$


Fig. 13. $\mathrm{d}\sigma/\mathrm{d}x_{\mathrm{LL}}^{\gamma}$ with the hadron and jet rapidity cuts $1 \le \eta^{h}, \eta^{\mathrm{jet}} \le 3$

the resolved contribution. The AFG02 parton distributions for the photon allow one to modify the normalisation of the non-perturbative VDM component. In order to

exhibit the sensitivity to this component, we show a curve where the coefficient of this VDM input has been set to zero. We also show the magnitude of the gluon contribution to $\mathrm{d}\sigma/\mathrm{d}x_{\mathrm{LL}}^{\gamma}$ in this kinematic range. We conclude from Fig. 13 that the rapidity cuts $1 \le \eta^{h}, \eta^{\mathrm{jet}} \le 3$ select a kinematic region where the sensitivity of the hadron-jet cross section to the gluon distribution in the photon is very large.

The contribution of the gluon in the proton turns out to be large even with rapidities integrated in the whole range $-2 \le \eta^{h,\mathrm{jet}} \le 2$, as can be seen from Fig. 14. We also observe that the effect of using different parton distributions for the proton, namely the MRST99 [24], the new MRST01 [25] and the CTEQ6M [26] sets, is quite large and mainly due to the different shapes of the gluons in the different sets. Although the variation of the cross section when varying all scales simultaneously between $0.3 \le C \le 2$ is larger than the variation due to the different pdf sets, the scale variations rather produce an overall shift of the curve, but do not change the shape. On the other hand, the fact that the gluon distribution of MRST01 peaks at higher x values than the one of CTEQ6M (see Fig. 16 of [26]) is clearly reflected in Fig. 14. We also note that the region $x_{\mathrm{LL}}^{p} \approx 0.02$, corresponding to $x_{\mathrm{parton}}^{p} \approx 0.05$, is an interesting x-range, because it lies in the window between constraints from HERA for lower x and the Tevatron jet data for higher x. Therefore the cross section $\mathrm{d}\sigma/\mathrm{d}x_{\mathrm{LL}}^{p}$ can serve to further constrain the parton distributions of the proton.
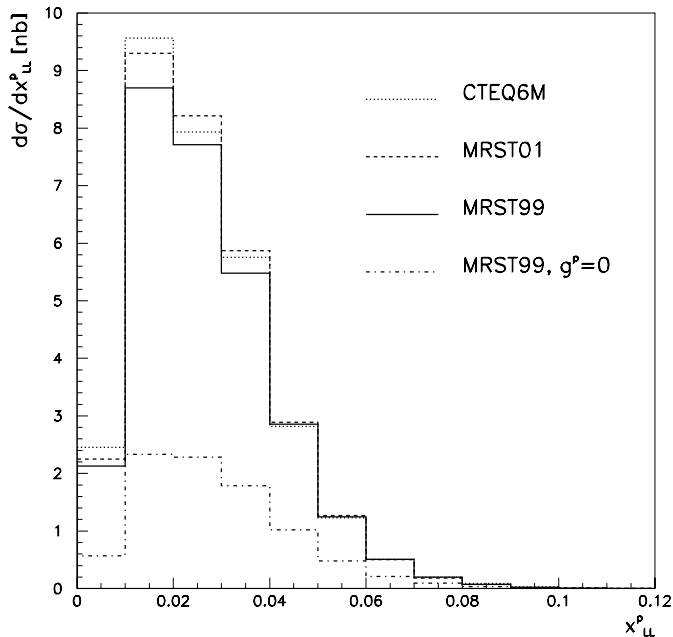
Fig. 14. $d\sigma/dx^p_{LL}$ calculated with different pdf sets and sizes of the gluon in the proton; rapidities integrated over the range $-2 \le \eta^{h,\text{jet}} \le 2$

5 Conclusion

We have studied the photoproduction of inclusive large p_T charged hadrons and the production of a charged hadron plus a jet. For the inclusive case we compared the p_T- and rapidity distributions to H1 data [11] and found reasonable agreement. However, for a value of $p_T^{\min}$ as low as 3 GeV, the dependence of the NLO result on the renormalisation and factorisation scales is very large. Only for $p_T^{\min} \gtrsim 7$ GeV a plateau where the cross section is approximately stable against scale variations could be found. We also studied the effect of using different fragmentation function parametrisations [7–9] and compared to a previous analysis of Kniehl, Kramer and Pötter [10]. For the parton distributions in the photon, we used the new AFG02 parametrisations [14].

For the hadron-jet cross section, we studied the rapidity distributions and the cross sections $d\sigma/dx^p$, $d\sigma/dx^\gamma$. We analysed the difference between the partonic momentum fractions $x^{p,\gamma}_{\text{parton}}$ and the observables $x^{p,\gamma}_{\text{obs}}$ defined via the observed transverse momenta and rapidities of the hadron and the jet. We further proposed a variable $x^{p,\gamma}_{LL}$ which does not require the measurement of the jet transverse energy.

We also carried out an exhaustive study of the scale dependence. We found a stability region for the cross section integrated over $7\,\text{GeV} \le p_T^h \le 15\,\text{GeV}$, $E_T^{\text{jet}} > 5\,\text{GeV}$ and performed a scale optimisation.

Finally, we investigated the possibility to constrain the parton distributions (in particular the gluon distributions) in the photon and in the proton via the hadron-jet cross section. We show how rapidity cuts can increase the sensitivity to the gluon distributions in the photon. We also

found a rather large sensitivity to the parton distributions in the proton. We show a comparison of the MRST99 [24] distributions to the new MRST01 [25] and CTEQ6M [26] distributions.

References

1. H1 coll., S. Aid et al., Z. Phys. C **70**, 17 (1996)
2. ZEUS coll., J. Breitweg et al., Eur. Phys. J. C **4**, 591 (1998)
3. ZEUS coll., J. Breitweg et al., Phys. Lett. B **472**, 175 (2000)
4. H1 coll., C. Adloff et al., Eur. Phys. J. C **1**, 97 (1998)
5. ZEUS coll., J. Breitweg et al., Eur. Phys. J. C **11**, 35 (1999)
6. ZEUS coll., S. Chekanov et al., Phys. Lett. B **511**, 19 (2001)
7. S. Kretzer, Phys. Rev. D **62**, 054001 (2000)
8. B.A. Kniehl, G. Kramer, B. Pötter, Nucl. Phys. B **582**, 514 (2000)
9. L. Bourhis, M. Fontannaz, J. Ph. Guillet, M. Werlen, Eur. Phys. J. C **19**, 89 (2001)
10. B.A. Kniehl, G. Kramer, B. Pötter, Nucl. Phys. B **597**, 337 (2001)
11. H1 coll., C. Adloff et al., Eur. Phys. J. C **10**, 363 (1999)
12. M. Fontannaz, J. Ph. Guillet, G. Heinrich, Eur. Phys. J. C **21**, 303 (2001)
13. M. Fontannaz, J. Ph. Guillet, G. Heinrich, Eur. Phys. J. C **22**, 303 (2001)
14. P. Aurenche, M. Fontannaz, J. Ph. Guillet, paper in preparation
15. P. Aurenche, M. Fontannaz, J. Ph. Guillet, Z. Phys. C **64**, 621 (1999)
16. S. Kawabata, Comp. Phys. Comm. **88**, 309 (1995)
17. S. Catani, Y.L. Dokshitzer, M.H. Seymour, B.R. Webber, Nucl. Phys. B **406**, 187 (1999); S.D. Ellis, D.E. Soper, Phys. Rev. D **58**, 3160 (1993)
18. B.A. Kniehl, G. Kramer, Z. Phys. C **62**, 53 (1994)
19. J. Binnewies, B.A. Kniehl, G. Kramer, Phys. Rev. D **52**, 4947 (1995); J. Binnewies, B.A. Kniehl, G. Kramer, Phys. Rev. D **53**, 3573 (1996)
20. B.A. Kniehl, in Proceedings of the 1997 Ringberg Workshop on New Trends in HERA Physics
21. Fermilab E706 coll., L. Apanasevich et al., Phys. Rev. Lett. **81**, 2642 (1998)
22. T. Binoth, J. Ph. Guillet, E. Pilon, M. Werlen, Eur. Phys. J. C **24**, 245 (2002)
23. P.M. Stevenson, Phys. Rev. D **23**, 2916 (1981); P. Aurenche, R. Baier, M. Fontannaz, D. Schiff, Nucl. Phys. B **286**, 509 (1987)
24. A.D. Martin, R.G. Roberts, W.J. Stirling, R.S. Thorne, Eur. Phys. J. C **14**, 133 (2000)
25. A.D. Martin, R.G. Roberts, W.J. Stirling, R.S. Thorne, Eur. Phys. J. C **23**, 73 (2002)
26. J. Pumplin, D.R. Stump, J. Huston, H.L. Lai, P. Nadolsky, W.K. Tung, JHEP 0207, 012 (2002)